



# Delivery of pOXR1 through an injectable liposomal nanoparticle enhances spinal cord injury regeneration by alleviating oxidative stress

Jing Zhang<sup>a,1</sup>, Yao Li<sup>b,1</sup>, Jun Xiong<sup>a,1</sup>, Helin Xu<sup>a,1</sup>, Guanghen Xiang<sup>b</sup>, Mingqiao Fan<sup>b</sup>, Kailiang Zhou<sup>b</sup>, Yutian Lin<sup>a</sup>, Xiangxiang Chen<sup>a</sup>, Lin Xie<sup>a</sup>, Hongyu Zhang<sup>a</sup>, Jian Wang<sup>a,\*</sup>, Jian Xiao<sup>a,\*\*</sup>

<sup>a</sup> Department of Hand Surgery and Peripheral Neurosurgery, The First Affiliated Hospital and School of Pharmaceutical Sciences, Wenzhou Medical University, Wenzhou, 325025, China

<sup>b</sup> Department of Orthopaedics, The Second Affiliated Hospital and Yuying Children's Hospital of Wenzhou Medical University, Wenzhou, 325000, China

## ARTICLE INFO

### Keywords:

Gene therapy  
OXR1  
DNA condensed agent  
Spinal cord injury  
Oxidative stress

## ABSTRACT

Oxidation resistance 1 (OXR1) is regarded as a critical regulator of cellular homeostasis in response to oxidative stress. However, the role of OXR1 in the neuronal response to spinal cord injury (SCI) remains undefined. On the other hand, gene therapy for SCI has shown limited success to date due in part to the poor utility of conventional gene vectors. In this study, we evaluated the function of OXR1 in SCI and developed an available carrier for delivering the OXR1 plasmid (pOXR1). We found that OXR1 expression is remarkably increased after SCI and that this regulation is protective after SCI. Meanwhile, we assembled cationic nanoparticles with vitamin E succinate-grafted ε-polylysine (VES-g-PLL) (Nps). The pOXR1 was precompressed with Nps and then encapsulated into cationic liposomes. The particle size of pOXR1 was compressed to 58 nm, which suggests that pOXR1 can be encapsulated inside liposomes with high encapsulation efficiency and stability to enhance the transfection efficiency. The agarose gel results indicated that Nps-pOXR1-Lip eliminated the degradation of DNA by DNase I and maintained its activity, and the cytotoxicity results indicated that pOXR1 was successfully transported into cells and exhibited lower cytotoxicity. Finally, Nps-pOXR1-Lip promoted functional recovery by alleviating neuronal apoptosis, attenuating oxidative stress and inhibiting inflammation. Therefore, our study provides considerable evidence that OXR1 is a beneficial factor in resistance to SCI and that Nps-Lip-pOXR1 exerts therapeutic effects in acute traumatic SCI.

## 1. Introduction

Traumatic spinal cord injury (SCI) is a devastating condition that results in long-term disability and death worldwide [1]. Neuronal cell death is one of the most critical pathological issues caused by direct mechanical impact, followed by a series of secondary molecular cascades, including mitochondrial damage, reactive oxygen species (ROS) and misfolded protein accumulation, and the inflammatory response [2–4]. Although neural tissue is associated with limited intrinsic regenerative capability, increasing evidence indicates that targeting these secondary molecular processes is a therapeutic method for

improving functional recovery after SCI in many animal cases [5–7].

During SCI, excessive ROS accumulate and disrupt redox homeostasis. This pathological process results in cellular organelle damage and oxidative cell death [7,8]. Intriguingly, as a highly conserved protein in many eukaryotic organisms, oxidation resistance 1 (OXR1), was originally discovered as a protective agent capable of inhibiting oxidative DNA damage and subsequently believed to be related to the modulation of the antioxidant defense system by activating its target gene [9,10]. In addition, OXR1 has emerged as a critical regulator in neuronal cell development and function, and loss of OXR1 results in oxidative cell death in cerebellar granule neurons and is associated with several

Peer review under responsibility of KeAi Communications Co., Ltd.

\* Corresponding author. Department of Hand Surgery and Peripheral Neurosurgery, The First Affiliated Hospital, Wenzhou Medical University, Wenzhou, 325035, China.

\*\* Corresponding author. School of Pharmaceutical Science, Wenzhou Medical University, Wenzhou, 325035, China.

E-mail addresses: [jianwang0516@wmu.edu.cn](mailto:jianwang0516@wmu.edu.cn) (J. Wang), [xjian@wmu.edu.cn](mailto:xjian@wmu.edu.cn) (J. Xiao).

<sup>1</sup> These authors contribute equally to this study.

<https://doi.org/10.1016/j.bioactmat.2021.03.001>

Received 27 December 2020; Received in revised form 17 February 2021; Accepted 2 March 2021

2452-199X/© 2021 The Authors. Publishing services by Elsevier B.V. on behalf of KeAi Communications Co. Ltd. This is an open access article under the CC

BY-NC-ND license (<http://creativecommons.org/licenses/by-nc-nd/4.0/>).

neurological disorders, including epilepsy, deafness and mental retardation [11]. Correspondingly, promoting OXR1 expression has been shown to improve the pathological conditions of Alzheimer's disease and Parkinson's disease [12,13]. Furthermore, modulation of OXR1 has also been reported to be beneficial for pulmonary arterial hypertension and kidney injury [14]. Importantly, OXR1 is expressed in neurons of the spinal cord, and overexpression of OXR1 contributes to preventing the progression of amyotrophic lateral sclerosis [11,15]. However, the effects of OXR1 in the regulation of traumatic neural injury remain unclear.

Although numerous molecular targets have been identified as advantageous factors for treatment, most related methods, including gene knockdown or virus delivery, are unavailable in clinical cases, especially for molecules without specific inhibitors or activators. Therefore, discovering an effective and safe vehicle as a gene therapy tool would be helpful for the treatment of SCI. Plasmids are accessible tools for modulating molecule expression, delivering plasmids using biological materials could enhance plasmid efficiency, concentration and biological stability [16]. In particular, liposome-based nanoparticles are known to be good carriers for the loading, transport and release of plasmids to their target [17,18]. Consistent with previous studies, a novel liposome modified with vitamin E and natural poly  $\epsilon$ -lysine ( $\epsilon$ -PLL) was constructed to simultaneously encapsulate the OXR1-EGFP fusion plasmid (pOXR1) [19,20].  $\epsilon$ -PLL can effectively condense plasmid DNA at high concentrations, similar to polyethylenimine (PEI) [21], which is a common DNA transfection lipophilicity material, whereas  $\epsilon$ -PLL is associated with biodegradability and reduced toxicity compared to PEI.

The aim of the current investigation was to synthesize a liposomal nanocarrier using vitamin E succinate-grafted  $\epsilon$ -polylysine (VES-g-PLL) as the backbone and pOXR1 to evaluate its protective effect in oxidative stress in experimental traumatic SCI. In the current study, VES-g-PLL was simultaneously assembled into a cationic micelle with a proper hydrodynamic diameter and zeta potential, and pOXR1 was condensed by the VES-g-PLL complex and loaded in the inner aqueous compartment of liposomes with considerable stability and capability. Moreover, this loading complex effectively attenuated oxidative stress and promoted functional recovery after SCI. Therefore, our results indicate that the VES-g-PLL-pOXR1 nanoparticle represents a potential candidate for the management of SCI.

## 2. Materials and methods

### 2.1. Reagents and antibodies

The recombinant OXR1-EGFP fusion plasmid was constructed by GeneChem (Shanghai, China). Egg lecithin (PC-98T) and synthetic phospholipids (DSPE-PEG2000) were provided by RVT (Shanghai, China). Cholesterol, N-hydroxy-succinimide (NHS), N-(3-dimethylaminopropyl)-N'-ethyl carbodiimide hydrochloride (EDC),  $\epsilon$ -polylysine and d- $\alpha$ -tocopherol succinate were purchased from Sigma (Saint Louis, MO, USA). Fetal bovine serum (FBS) was provided by PAN-Biotech GmbH (Baghlia, Germany). PEI was purchased from Thermo Scientific (Madison, WI, USA). RPMI 1640 medium, penicillin/streptomycin solution, and neurobasal medium were purchased from Gibco (CA, USA). The MTT Cell Proliferation and Cytotoxicity Assay Kit, HE staining kit and Masson staining kit were obtained from Solarbio Science & Technology (Beijing, China). A TUNEL apoptosis detection kit was obtained from Yeasen Biochemical (Shanghai, China). Primary antibodies and the companies from which they were obtained are listed in [Supplemental Table 1](#). Alexa Fluor 568, Alexa Fluor 488 and Alexa Fluor 647 donkey anti-rabbit/mouse secondary antibodies against mouse and rabbit were purchased from Abcam (Cambridge, UK).

### 2.2. Preparation of VES-g-PLL nanoparticles

Synthesis of VES-g-PLL polymers is primarily based on the condensation reaction between the carboxyl group of VES and the amino group of  $\epsilon$ -PLL, and we can adjust the VES/ $\epsilon$ -PLL ratios to obtain polymers with different VES graft ratios. VES-g-PLL was synthesized by a previously reported method [22]. Briefly,  $\epsilon$ -PLL (1 g) was dissolved in 30 mL DMSO, and the carboxyl group of VES was activated in DMSO in the presence of EDC and NHS (VES, EDC and NHS, molar ratio of 1:1:1). Activated VES was added dropwise to the  $\epsilon$ -PLL solution, reacting for 24 h under stirring at room temperature. Then, the whole reaction solution was placed into dialysis bags (MW cut off of 3500 Da), dialyzed against 50% ethanol for 48 h, distilled water for 24 h, and lyophilized.

### 2.3. Fabrication of Nps-pOXR1-Lip

First, pDNA-loaded VES-g-PLL nanoparticles were prepared by mixing a pDNA solution (10  $\mu$ g/ $\mu$ L) in VES-g-PLL micelles. Nps-pOXR1-Lip was prepared by the reverse-phase evaporation method according to a previous publication with some modifications [19]. Briefly, 5 mg DSPE-PEG2000, 85 mg PC-98T and 10 mg cholesterol were dissolved in 10 mL of dichloromethane as the oil phase. Then, Nps-pOXR1 was gradually added into the oil phase and emulsified to prepare a W/O-type emulsion under a probe ultrasonic instrument (Branson 450 Sonifier, 60 s, 50 W amplitude, 3 s, off 3 s). Next, the organic solvent was evaporated by rotary evaporators under vacuum at 37 °C to form a dry film. Then, the dry film in the bottle wall was hydrated with pH 7.4 PBS at room temperature followed by homogenization using probe ultrasonication (50 W amplitude, 10 min, 3 s, off 3 s) in an ice bath to obtain Nps-pOXR1-Lip.

### 2.4. Characterization of Nps-pOXR1-Lip

Size and zeta potential were determined using dynamic light scattering (DLS) measurements (Litesizer, Anton Paar, Austria) at a laser beam wavelength of 632.8 nm and a scattering angle of 90° at 25 °C. Morphology was imaged under transmission electron microscopy (JEOLJEM-2000EX, JEOL, Japan) with phosphotungstate acid solution (2%, w/w) staining. A gel retardation assay was used to detect the encapsulating efficiency of pDNA. Briefly, complexes including pOXR1 at various mass ratios of liposome-polymer were centrifuged at 12000 rpm for 1 h, and then 8  $\mu$ L of supernatant was mixed with 2  $\mu$ L of 10 $\times$  loading buffer. The samples were electrophoresed on a 1% (w/v) agarose gel for 90 min at 80 V. The resulting gels were imaged under a UV illuminator gel documentation system (Bio-Rad, Hercules, CA). Alternatively, Triton X-100 (10%) was used to break the liposome shell, and then the mixtures were separately incubated with PBS containing heparin (12  $\mu$ L, 5 mg/mL) for 60 min of incubation at 37 °C to dissociate pDNA from VES-g-PLL. All formulations were centrifuged for 1 h (12000 rpm, 4 °C), and then the supernatant was qualitatively analyzed by agarose gel electrophoresis.

### 2.5. Physicochemical stability of Nps-pOXR1-Lip

Nps-pOXR1-Lip was incubated with Ph6.5 PBS containing 10% human serum albumin at 37 °C. Then, the particle size and particle size distribution (PDI) were detected by DLS at each time point to evaluate its stability. DNase I was utilized to investigate the efficiency of Nps-Lip in protecting pDNA from degradation. First, Nps-pOXR1-Lip was incubated with DNase I reaction buffer (3  $\mu$ L, 1 U/ $\mu$ L) at 37 °C for 30 min, and then the reaction was stopped by the addition of ethylenediaminetetraacetic acid (EDTA, 5  $\mu$ L, 100 mM/ $\mu$ L) at room temperature. Next, the mixture was treated with Triton X-100 (10%) and heparin and then centrifuged. The supernatant was detected by an agarose gel.

## 2.6. Cell culture

PC12 cells, a commonly used nerve cell line, were provided by the Cell Storage Center of Wuhan University (Wuhan, China) and induced to differentiate into neuron-like cells by NGF (50 ng/mL) treatment for 3 days. Cells were incubated in a humidified incubator in RPMI 1640 medium with 1% penicillin-streptomycin-glutamine solution and 10% FBS at 37 °C and 5% CO<sub>2</sub>.

## 2.7. Cytotoxicity evaluation

The cytotoxicity of the polymer, polymer/lip complex and PEI was assessed by the MTT method. PC12 cells were seeded into 96-well plates ( $8 \times 10^3$  cells per well) and incubated with complete medium. After 24 h, cells were incubated with fresh medium containing various concentrations of materials for 24 h. Then, the medium was removed, and 10  $\mu$ L MTT solution was added to each well and cultured for 4 hours. The medium was replaced with 100  $\mu$ L of DMSO, and the 96-well plates were measured at a wavelength of 490 nm by a microplate reader (MultiskanMK3, Thermo, USA). PEI (Invitrogen), a marketed product, was used as a control.

## 2.8. Transfection assay in vitro

Transfection efficiency was investigated in PC12 cells by detecting the fluorescence intensity of the OXR1-EGFP fusion plasmid (pDNA), which was encapsulated in the polymer/lip complex and PEI. Briefly, PC12 cells were seeded in 6-well tissue culture plates at a density of  $1 \times 10^4$  cells per well and cultured for 24 h. Then, the complexes were added to PC12 cells for 24 h. Meanwhile, PEI-pOXR1 and naked pOXR1 were used as positive and negative controls, respectively.

## 2.9. Animal contusive spinal cord injury model

Adult female Sprague-Dawley rats (250–300 g) were approved for use by the Animal Center of the Chinese Academy of Science (Shanghai, China). All animal experiments were approved by the Laboratory Animal Ethics Committee of Wenzhou Medical University. The total number of adult female Sprague-Dawley rats are 286, sham group (n = 16), SCI group (n = 90), pOXR1, Nps-pOXR1, Nps-pOXR1-Lip group (n = 180) and kept under controlled environmental conditions. Establishment of the model was performed as previously described [23]. Behavioral tests were performed on all rats one day before surgery to evaluate hind limb function. Briefly, all rats were anesthetized with 8% (w/v) chloral hydrate (3.5 mL/kg, i.p.). After the corneal reflex stopped, the surgical site was shaved, and the skin was disinfected with iodine and 70% ethanol. Then, layers of the skin and paravertebral muscles in the back of the rats were cut, and a laminectomy was performed at the T9–T10 vertebra. The spinal cord was fully exposed and contused from a height of 50 mm with the MASCIS impinge (W.M. Keck Center for Collaborative Neuroscience Rutgers, The State University of New Jersey, USA). The epidural membrane between T9 and T10 was picked up with a 32-syringe needle, and the wound was enlarged with microscopic scissors to completely expose the dorsal side of the spinal cord. A Hamilton microinjector was used to inject drug on the exposed spinal cord surface. Then, muscle and skin were sutured, all rats received 0.5 mL of normal saline and were returned to a warm blanket for postoperative recovery, and then kept in a warm cage and given free access to food and water. The bladder was manually evacuated twice one day until the restoration of the urinating function.

## 2.10. Functional behavior assessment

Rats were continuously given BBB (Basso, Beattie, and Bresnahan Loco Motor Rating Scale) behavioral scores and inclined plane tests at –1, 0, 3, 7, 14, 21 and 28 days after modeling. *BBB test*: rats were placed

in an open field, and two observers stood opposite to observe the buttocks, knees, bare joints, walking, trunk movement and coordination of the rats. The observer rated the score on a scale from 0 to 21. *Inclined plane test*: The rats were placed on a board with a rubber surface. As the board angle increased, the maximum angle was recorded and defined as the value at which the mouse could not hold its position for 5 s without falling. Each mouse was evaluated three times and allowed to rest for 1 min between tests. *Footprint analysis*: footprint analysis was performed by immersing the animal's hind paws in red dye, as described previously [24]. Rats were allowed to walk on a straight strip of white paper (100 cm in length and 10 cm in width), and then their footprints were scanned and analyzed.

## 2.11. Tissue preparation

Spinal cord tissues at the specified time points were obtained after euthanizing rats with an overdose of 8% (w/v) sodium pentobarbital (40 mg/kg) and ventricular perfusion with normal saline. For western blot and staining, rats were perfused with 4% paraformaldehyde (PFA) after normal saline ventricular perfusion. The 1 cm long spinal cord tissue at the center of the injury was then dissected and fixed in 4% paraformaldehyde at 4 °C for 24 h. After fixation, the spinal cord was dehydrated, paraffin-embedded, and then sectioned (5  $\mu$ m) longitudinally and transversally. Sections were subsequently mounted on slides for subsequent staining.

## 2.12. Western blot assay

Protein samples were extracted from PC12 cells or animal tissues and quantified using a BCA protein assay kit (Thermo Fisher Scientific Inc., Waltham, MA). Equivalent amounts of protein (60  $\mu$ g) were separated by SDS polyacrylamide gel electrophoresis and then transferred to polyvinylidene fluoride (PVDF) membranes. The membranes were blocked for 1.5 h in 5% skimmed milk and then incubated with the primary antibody at 4 °C overnight. On the second day, membranes were incubated with HRP-conjugated IgG secondary antibody at room temperature for 1 h after washing with TBST 3 times. Finally, band intensities were detected using a ChemiDc™ XRS + Imaging System (Bio-Rad).

## 2.13. Immunofluorescence (IF) and histology staining

Paraffin sections, frozen sections of the spinal cord and PC12 cell slides were prepared for IF [25]. The samples were dewaxed and rehydrated, blocked in 5% bovine serum albumin and incubated at 4 °C overnight with the primary antibodies. Next, sections were washed with PBST and then incubated with secondary antibodies. Nuclei were labeled with DAPI for 5 minutes, and images were obtained using a Nikon ECLIPSE80i microscope (Tokyo, Japan). HE staining is commonly used to evaluate cellular and extracellular matrix characteristics, and Masson staining is used to measure collagen deposition at the site of injury.

## 2.14. Statistical analysis

All data are reported as the mean  $\pm$  standard deviation obtained from at least three independent results and were statistically analyzed by GraphPad Prism (version 8.0) or Origin software (version 2019b). Pairwise comparisons between two groups were determined using Student's t-test. For multiple groups, one-way analysis of variance (ANOVA) was used, followed by Tukey's test for pairwise comparisons of multiple groups. A P-value less than 0.05 was considered statistically significant.

### 3. Results

#### 3.1. OXR1 expression is increased in injured neurons

To evaluate OXR1 expression in neurons in the spinal cord, OXR1 levels were detected over time after traumatic injury. Initially, using western blot, OXR1 expression was obviously increased 1 day and 3 day after injury (Fig. 1a and b). Furthermore, co-IF results showed that the increased OXR1 protein was primarily localized in the neurons of the spinal cord (Fig. 1c and d). Because oxidative stress is one of the most common and critical secondary molecular processes in SCI, we further reasoned that oxidative stress may affect OXR1 expression. Employing cultured PC12 cells, western blot results showed that TBHP, a well-established ROS donor, enhanced OXR1 expression and peaked at 6 h

after stimulation (Fig. 1e and f). Collectively, these results suggested that OXR1 is increased after injury and may be related to neuroprotection.

#### 3.2. Preparation and characterization of Nps-pOXR1-Lip

According to our previous study, nanoparticles with a size of approximately 20 nm easily self-assemble into VES-g-PLL micelles in water [20]. Furthermore, because of its cellular penetration and extremely high positive properties, VES-g-PLL is regarded as a very promising DNA nonviral vector. In our study, nanoparticles assembled from VES-g-PLL polymers were used to condense pOXR1, and then polymers/DNA complexes were further encapsulated into liposomes (Fig. 2a). DNA compression enhances the physicochemical stability and

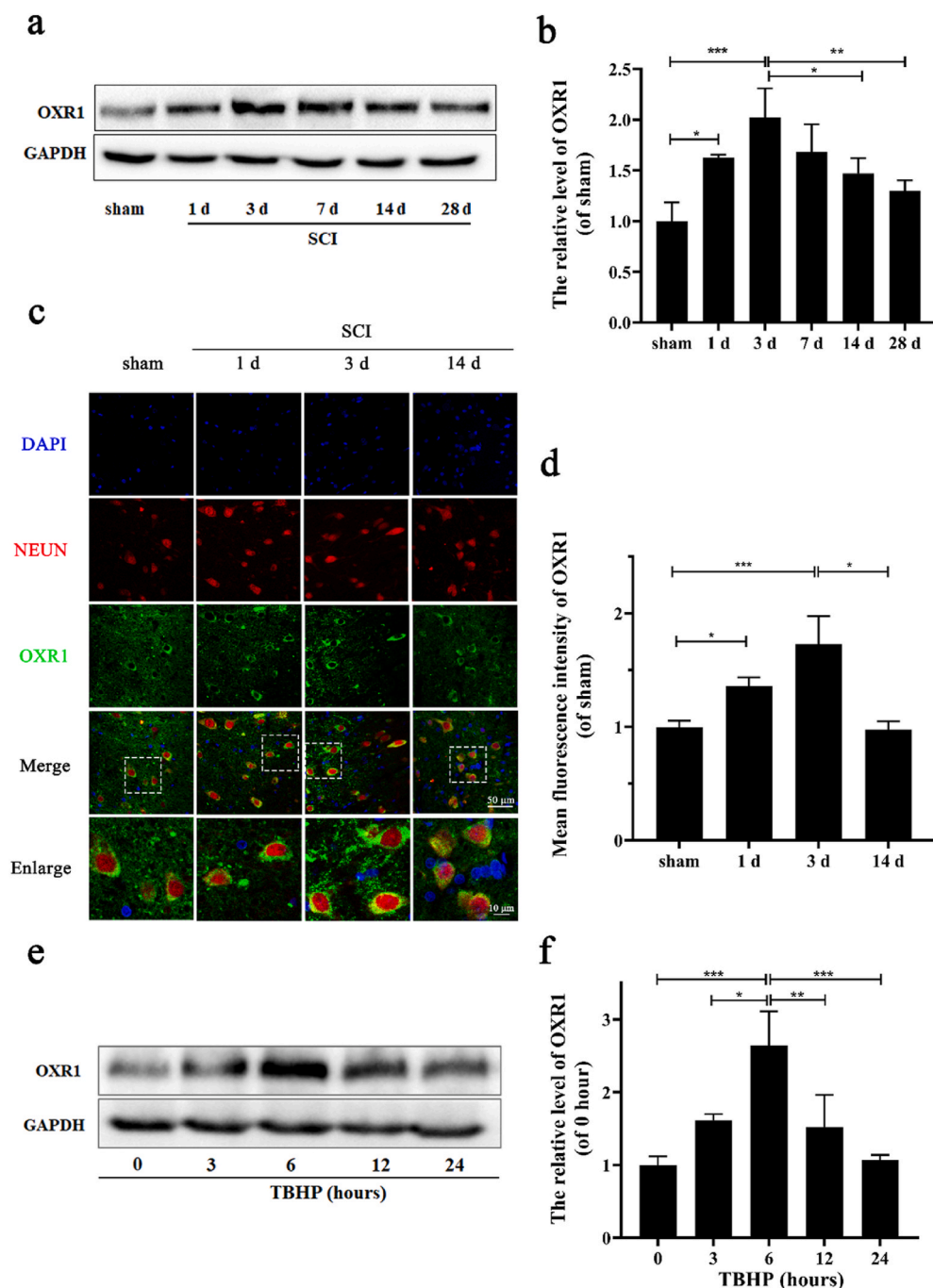


**Fig. 1.** Expression of OXR1 is increased in neurons in vivo and in vitro following injury. (a–b) Representative western blotting and quantification of OXR1 protein in spinal cord at specified times after SCI. (c–d) Immunofluorescence staining and quantitative analysis of OXR1 expression in neurons in the indicated groups after SCI. Scale bar = 50 μm. Scale bar (Enlarged) = 10 μm. (e–f) Immunoblots and quantification of TBHP-subjected PC12 cells at different time points. GAPDH was the loading control. Data are presented as the means ± SD, n = 3. Significant differences among the different groups are indicated by \*p < 0.05, \*\*p < 0.01, \*\*\*p < 0.001. Sham was used as a control.

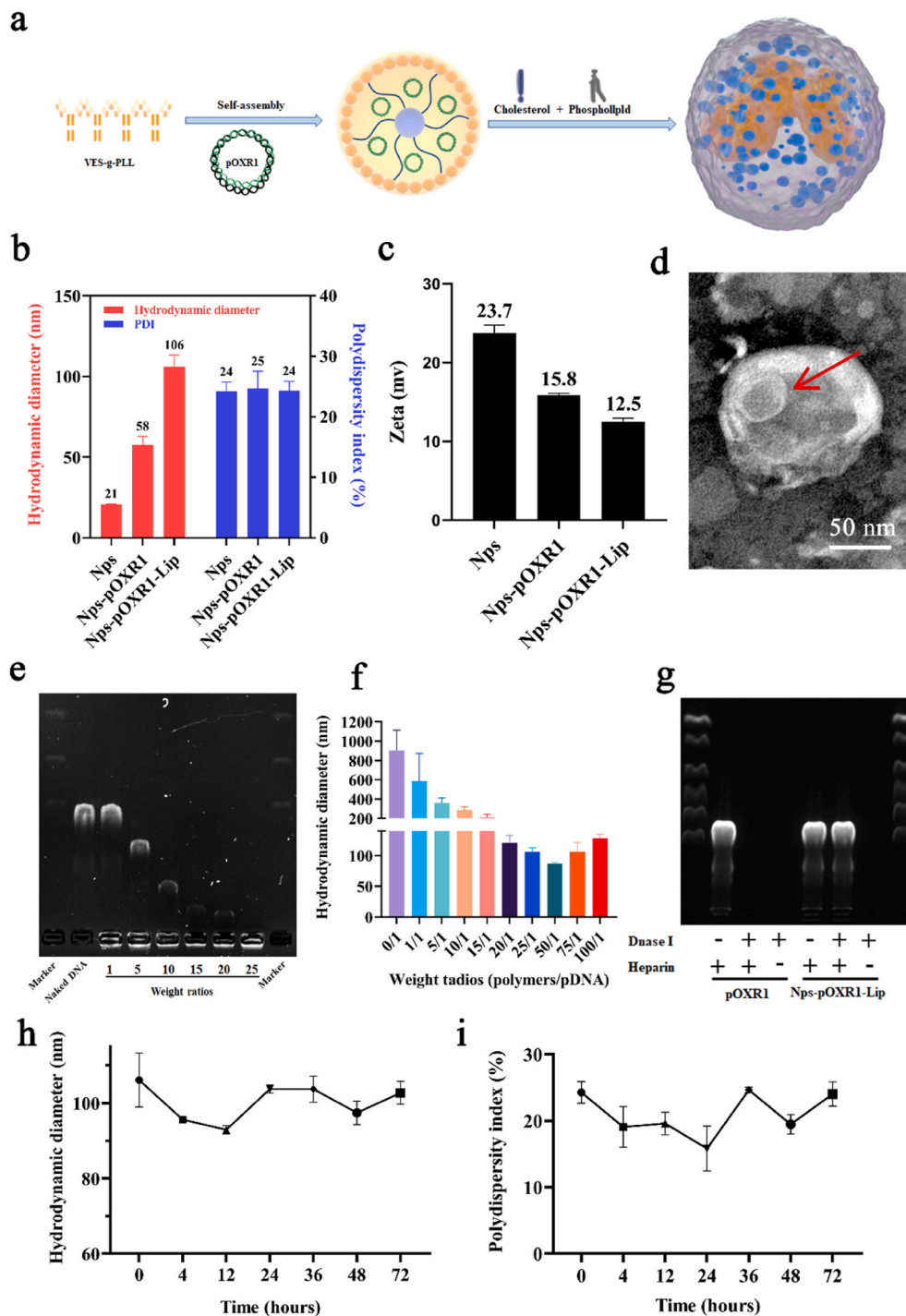


**Fig. 2.** Characterization of Nps-pOXR1-Lip. (a) Schematic diagram of the production process of Nps-pOXR1-Lip. (b) Transmission electron microscopy images of Nps-pOXR1-Lip. Scale bars = 50 nm. (c) Hydrodynamic diameter, PDI and (d) Zeta of Nps, Nps-pOXR1, Nps-pOXR1-Lip. n = 3. (e) Gel retardation assay of Nps-pOXR1-Lip prepared at varying weight ratios. (f) Hydrodynamic diameter of Nps-pOXR1-Lip at various weight ratios. n = 3. (g) Gel retardation assay of Nps-pOXR1-Lip incubated with DNase I. (h) At specified points, the hydrodynamic diameter and (i) PDI of Nps-pOXR1-Lip incubated with pH 6.5 PBS containing 10% human serum albumin at 37 °C was detected by DLS. n = 3.

transfection efficiency of liposome complexes [26]. As DLS data revealed, the size of pDNA was compressed from 800 nm to 57.6 nm and particle size distributed evenly (PDI = 0.24) (Fig. 2b). It meant that precompression were beneficial to encapsulate more DNA into liposome to enhance the encapsulation efficiency of liposome. Accordingly, the zeta potential of Nps decreased from 23.7 mV to 15.8 mV which showed that negatively charged DNA has bonded to the polymers (Fig. 2c). Technically, Nps-pOXR1 compounds were encapsulated into the aqueous compartment of liposomes by the reverse-phase evaporation technique, which is beneficial for reducing the cytotoxicity of Nps. Transmission electron microscopy (TEM) showed that Nps-pOXR1-Lip exhibited the spherical morphology and some tiny aggregate of

Nps-pOXR1 (red arrow) were dispersed inside of liposome. It indicated that Nps-pOXR1 complexes were successfully loaded into the liposome (Fig. 2d).

Gel retardation assays are widely used to determine the stability and encapsulation efficiency of gene carriers. The preparation of complexes/DNA is primarily based on electrostatic interactions between negatively charged DNA and positively charged polymers. As shown in Fig. 2e, the migration speed and distance of DNA in the complex were changed when the complex/DNA was fabricated with varying weight ratios of complex/DNA. This is due to partial or complete binding of DNA to cationic liposomes leading to slower electrophoresis speed, which is reflected in the short migration distance of DNA. In our study, free DNA

was rarely present on agarose gels when the weight ratio was  $\geq 25$ . The results showed that nucleic acids were completely encapsulated in the aqueous compartment of liposomes. In addition, the complex/DNA weight ratio also had an even stronger impact on the particle size of liposomes (Fig. 2f). Appropriate particle size is essential for effective gene transfection. Based on previous reports, the transfection effect is

best when the gene vector diameter is 100–200 nm [26]. The weight ratio of the vector used in the following study should be large enough to ensure that the DNA is completely wrapped. However, it is worth noting that the liposome complex, which is too stable, could be blocked in endosomes [27]; in contrast, its transfection efficiency is not enhanced. Deoxyribonuclease I (DNase I) is an endonuclease that digests single-

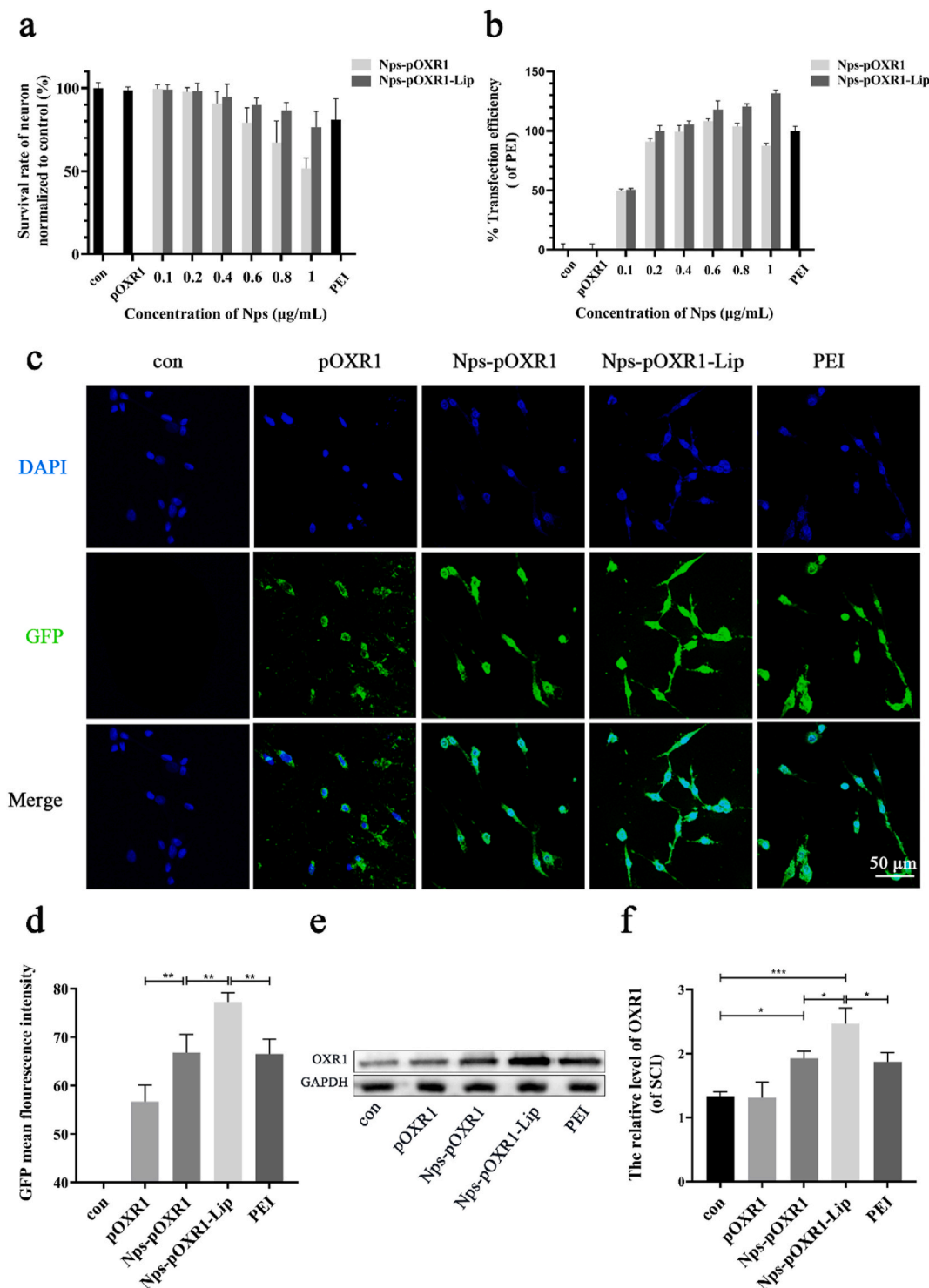


**Fig. 3.** In vitro cellular uptake and transfection assay. (a) Cell viability and (b) transfection efficiency of two types of complexes with different concentrations of Nps (VES-g-PLL micelle, concentration of VES-g-PLL in complexes) against PC12 cells after 24 h of incubation (n = 60). (c-d) Confocal images and quantitative analysis of PC12 cells after incubation with various compounds containing pDNA for 24 h. Scale bar = 50 μm (n = 3). (e-f) Immunoblots and quantification of OXRI protein in PC12 cells after the same treatment as above. PEI/pOXR1 (0.5 μg/mL) was used as a positive control. GAPDH was the loading control. Data represent mean ± SD. n = 6. \*p < 0.05, \*\*p < 0.01, \*\*\*p < 0.001.

or double-stranded DNA. Large quantities of DNase and other degrading enzymes are present in the tissue, cellular environment and blood as one of the main hindrances of gene transfection. Nps-pOXR1-Lip was incubated with DNase I to examine the efficiency of the liposomes in protecting pDNA from degradation. As shown in Fig. 2g, free pDNA was degraded; however, pDNA released from Nps-pOXR1-Lip by heparin was not digested by DNase I. After spinal cord injury, the tissue

microenvironment of lesions was slightly acidic [28]. Here, Nps-pOXR1-Lip was incubated with pH 6.5 PBS containing 10% HAS to determine the stability of liposomes in acidic environments. As shown in Fig. 2h and i, the hydrodynamic diameter and PDI of Nps-pOXR1-Lip did not change significantly in 72 h, which indicates that it has good stability in the weakly acidic SCI microenvironment.

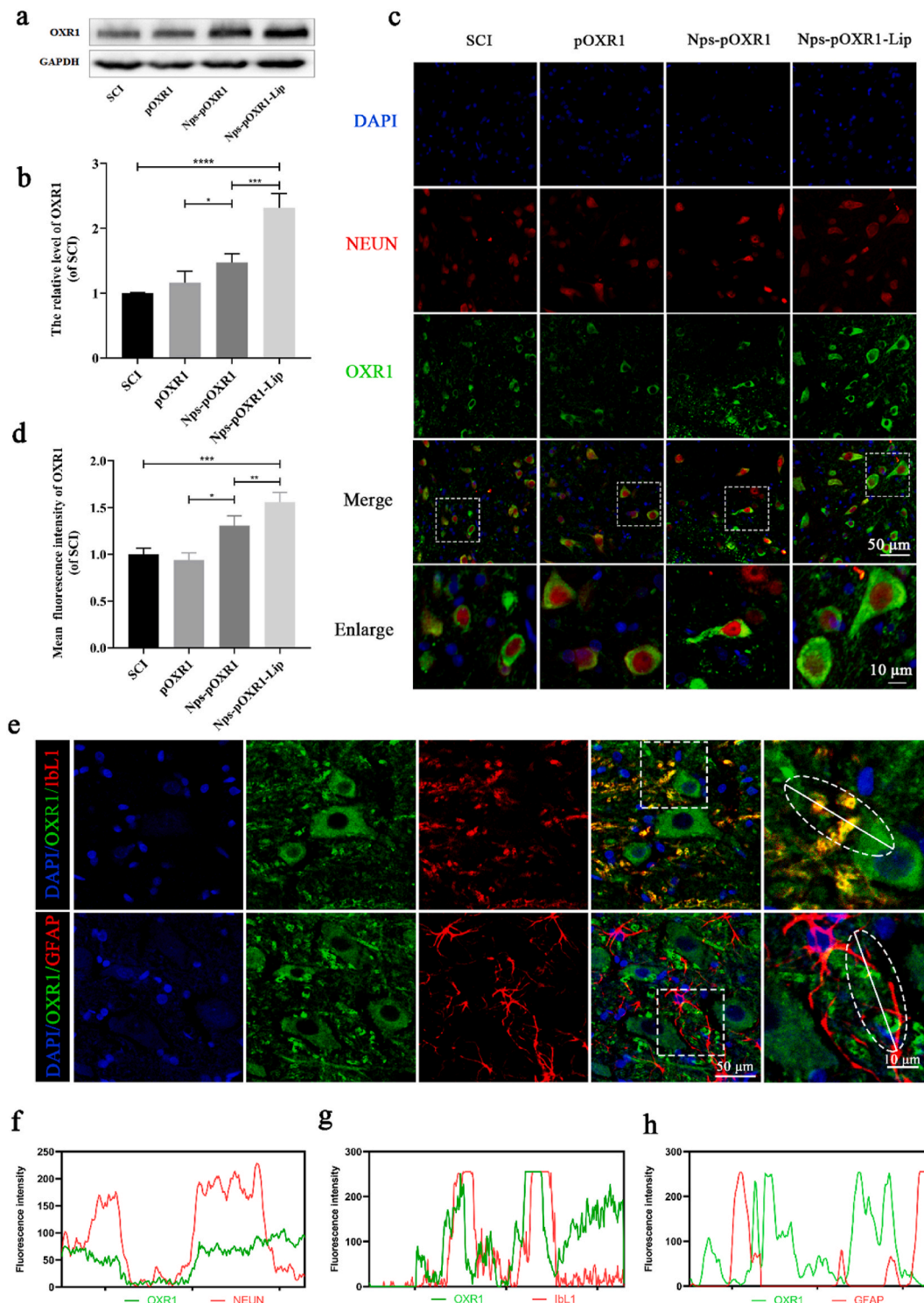


**Fig. 4.** Nps-pOXR1-Lip enhances OXR1 expression in the spinal cord. (a-d) Immunoblots and immunofluorescence staining of OXR1 in spinal cord tissues of rats after treatment with various formulations at 3 d. (e) Double immunostaining of OXR1 and GFAP or Iba1 at 3 d after SCI. (f-h) Immunofluorescence intensity of OXR1 and NEUN, GFAP and Iba1 across the white dotted lines in each group. Plot profile analysis in ImageJ was used to determine the colocalization of different indicators. Scale bar = 50  $\mu$ m. Scale bar (Enlarged) = 10  $\mu$ m. Data represent mean  $\pm$  SD. n = 3. \*p < 0.05, \*\*p < 0.01, \*\*\*p < 0.001.

3.3. Transfection efficiency and cytotoxicity of Nps-pOXR1-Lip in vitro

To explore the feasibility of Nps-pOXR1-Lip as a gene vector for neuron application, we assessed the cell viability and transfection efficiency of two types of complexes with different concentrations of Nps in

PC12 cells using PEI/DNA complexes as a positive control. As shown in Fig. 3a, the total complexes exerted dose-dependent cytotoxicity, and Nps-pOXR1 and PEI/DNA were more toxic than Nps-pOXR1-Lip at the same Nps concentration. The low cytotoxicity of Nps-pOXR1-Lip may be due to liposomes having a lower zeta potential than polymer complexes.

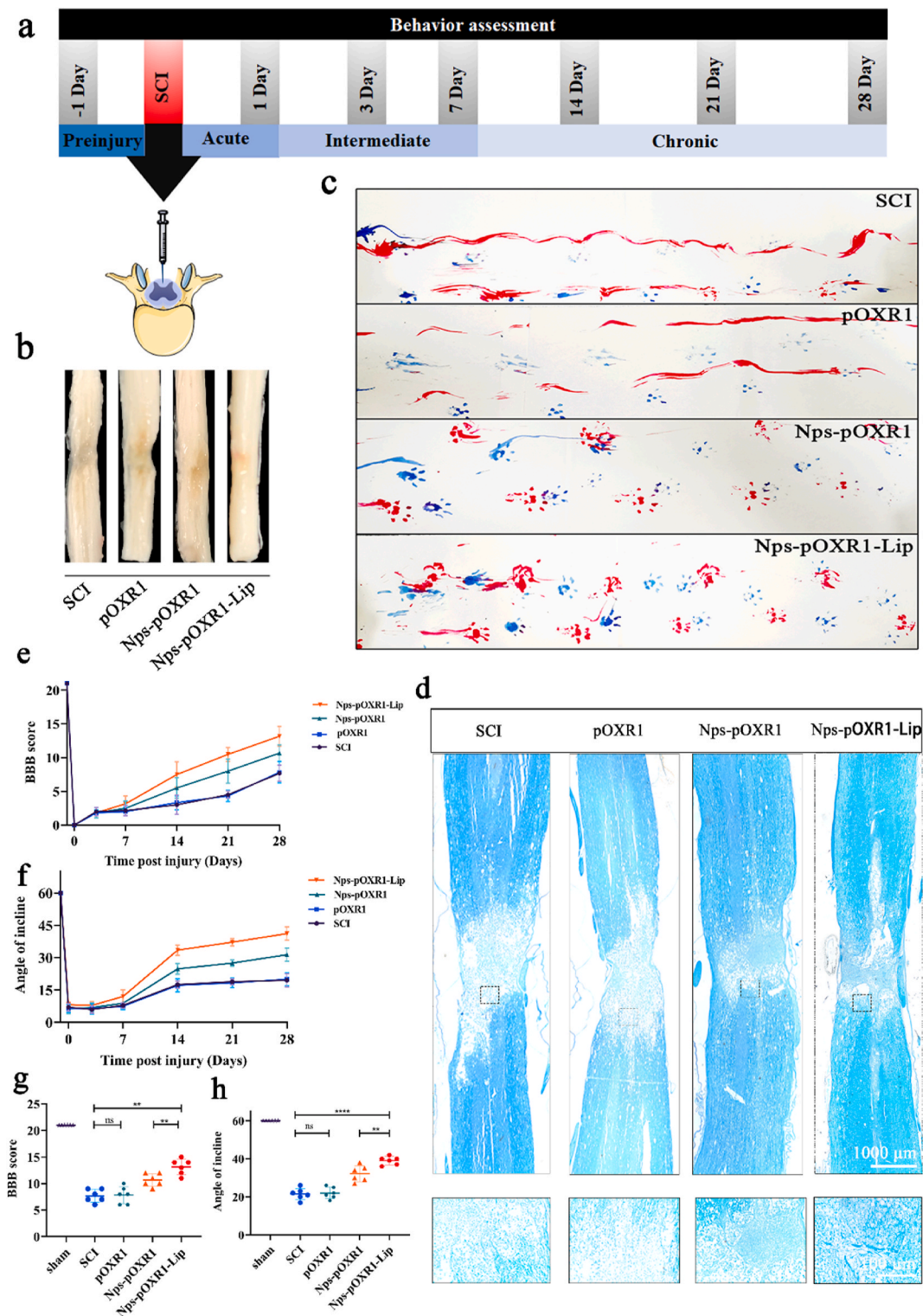
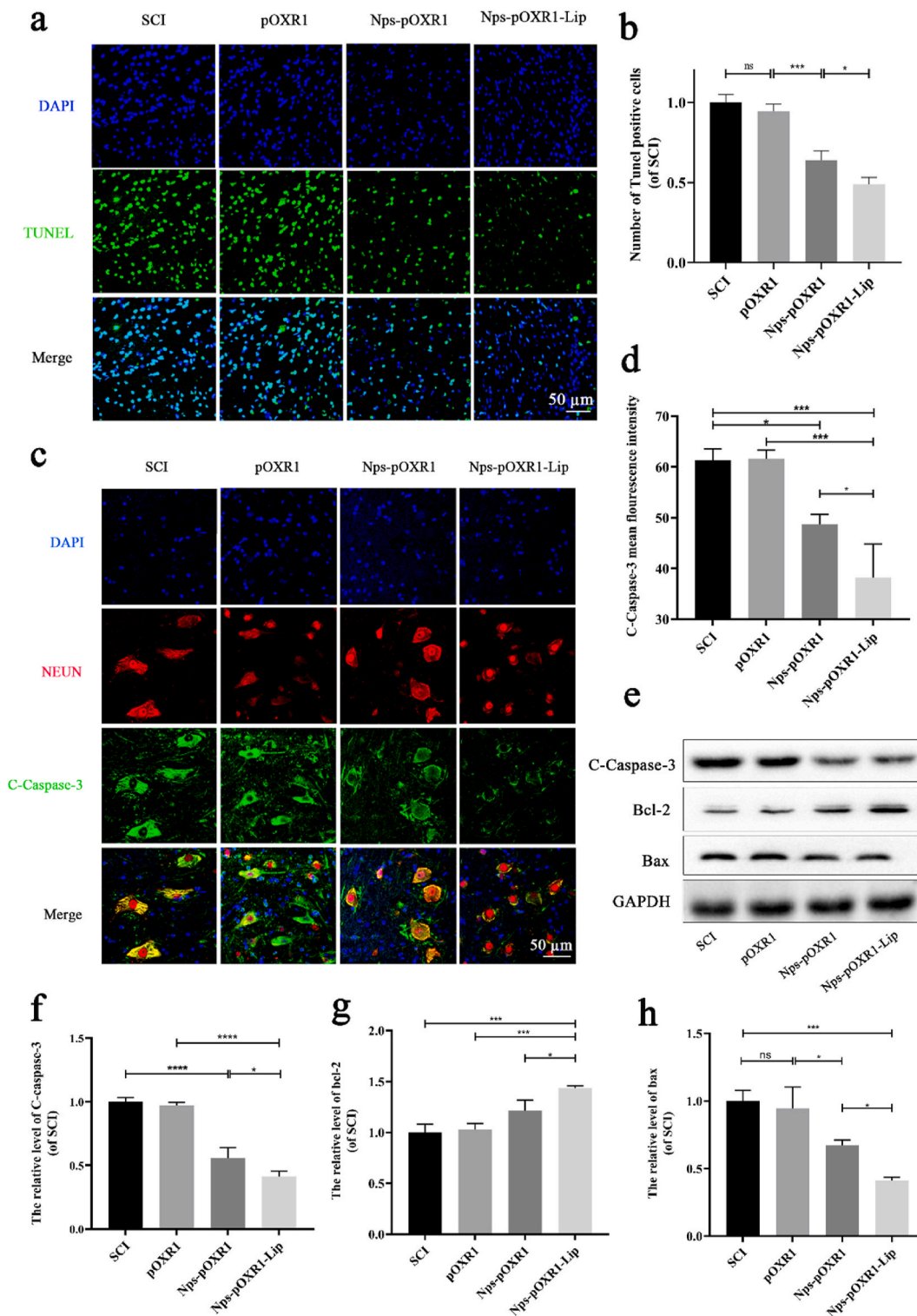


Fig. 5. Nps-pOXR1-Lip promotes functional recovery after SCI. (a) Drug injection model and behavioral experimental design. (b) Images of representative spinal cords of all treatment groups 28 days postinjury. (c) Footprint analysis of each group at 28 dpi (blue, forelimbs; red, hind limbs). (d) Representative images from LFB staining at 28 dpi. Scale bar = 1000 μm. Scale bar (Enlarged) = 100 μm. (e, g) Statistical analysis of the BBB in the different groups at -1, 1, 3, 7, 14, 21, and 28 dpi. n = 6. (f, h) Statistical analysis of the angle of inclined test in the different groups. n = 6. \*p < 0.05, \*\*p < 0.01, \*\*\*p < 0.001, \*\*\*\*p < 0.0001.

Therefore, Nps-pOXR1-Lip is a safe vehicle for pOXR1 loading when Nps are at a concentration of 0.8 μg/mL (cell survival rate ≥ 80%), which was selected for all subsequent experiments. In addition, the transfection efficiency of Nps-pOXR1-Lip was also determined. Compared to the control and Nps-pOXR1 groups, the Nps-pOXR1-Lip groups exhibited remarkably enhanced transfection efficiency (Fig. 3b). Meanwhile, the

GFP intensity of OXR1 was detected in vitro, and the Nps-pOXR1-Lip group exhibited much higher IF intensity (Fig. 3c and d). Similar to the above results, western blot also showed that the Nps-pOXR1-Lip group was associated with significantly increased OXR1 expression (Fig. 3e and f). Therefore, the assembled Nps-pOXR1-Lip is a safe and effective vehicle for increasing OXR1 expression.



**Fig. 6.** Nps-pOXR1-Lip reduces apoptosis after SCI. (a-b) Immunofluorescence staining and quantitative analysis of TUNEL in spinal cord sections from various groups at 7 dpi. Scale bar = 50 μm. (c-d) Confocal images of transverse spinal cord sections stained with OXR1 and C-caspase-3 at 7 dpi. Scale bar = 50 μm. (e-h) Immunoblots and quantification of C-caspase-3, Bcl-2, and Bax expression in rats after SCI in various groups. GAPDH was used as a loading control. Data represent mean ± SD. n = 3. \*p < 0.05, \*\*p < 0.01, \*\*\*p < 0.001, \*\*\*\*p < 0.0001.

3.4. Nps-pOXR1-Lip enhances OXR1 expression in the spinal cord

To further determine the efficiency of assembled Nps-pOXR1-Lip in vivo, OXR1 expression was also detected by western blot and IF in an animal model of SCI. As shown in (Fig. 4a and b), the Nps-pOXR1-Lip group presented a high level of OXR1 expression. In addition, the IF results also showed that Nps-pOXR1-Lip effectively enhanced OXR1

expression in spinal cord neurons (Fig. 4c and d). On the other hand, neuroinflammatory pathways in the spinal cord were alleviated by OXR1 overexpression [15]. We also evaluated whether Nps-pOXR1-Lip contributes to OXR1 expression in microglia and astroglial cells, which may also mediate relevant effects of SCI. IF results showed that there was no significant colocalization of OXR1 with GFAP, but colocalization of OXR1 with NEUN and Ibl1 was observed (Fig. 4e and f).

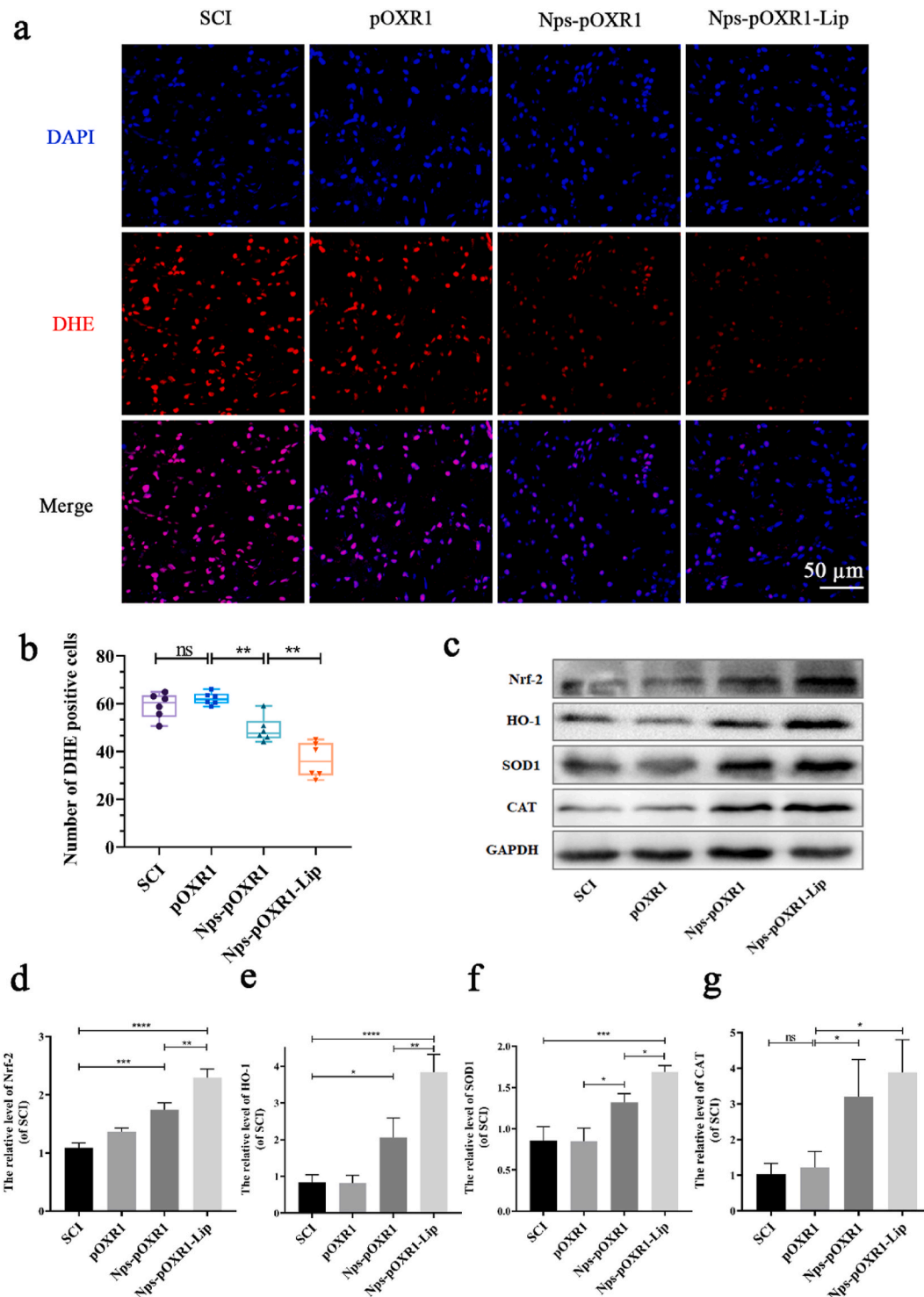


Fig. 7. Nps-pOXR1-Lip alleviates oxidative stress in vivo. (a-b) DHE staining for reactive ROS 3 days after SCI. Immunofluorescence and quantitative analysis of frozen spinal cord sections stained with DHE. Scale bar = 50  $\mu$ m. (c-g) Representative western blotting and quantification of Nrf-2, HO-1, SOD1, and CAT expression in rats after SCI in various groups at 3 dpi. GAPDH was the loading control. n = 3. Data represent mean  $\pm$  SD. n = 3. \*p < 0.05, \*\*p < 0.01, \*\*\*p < 0.001, \*\*\*\*p < 0.0001.

More, gene can express any protein or peptide by modifying the sequence of their bases, the protein is produced in a sustained manner, which can create long-lasting biological effects [17]. We further explored the sustained expression time of OXR1 after Nps-pOXR1-Lip injection, results showed that can maintain a higher expression at least 7 days in neurons (Figs. S1a–b). These data suggested

Nps-pOXR1-Lip is an effective vehicle for increasing neural OXR1 expression.

### 3.5. Nps-pOXR1-Lip promotes functional recovery after SCI

To evaluate the effect of Nps-pOXR1-Lip on the spinal cord after

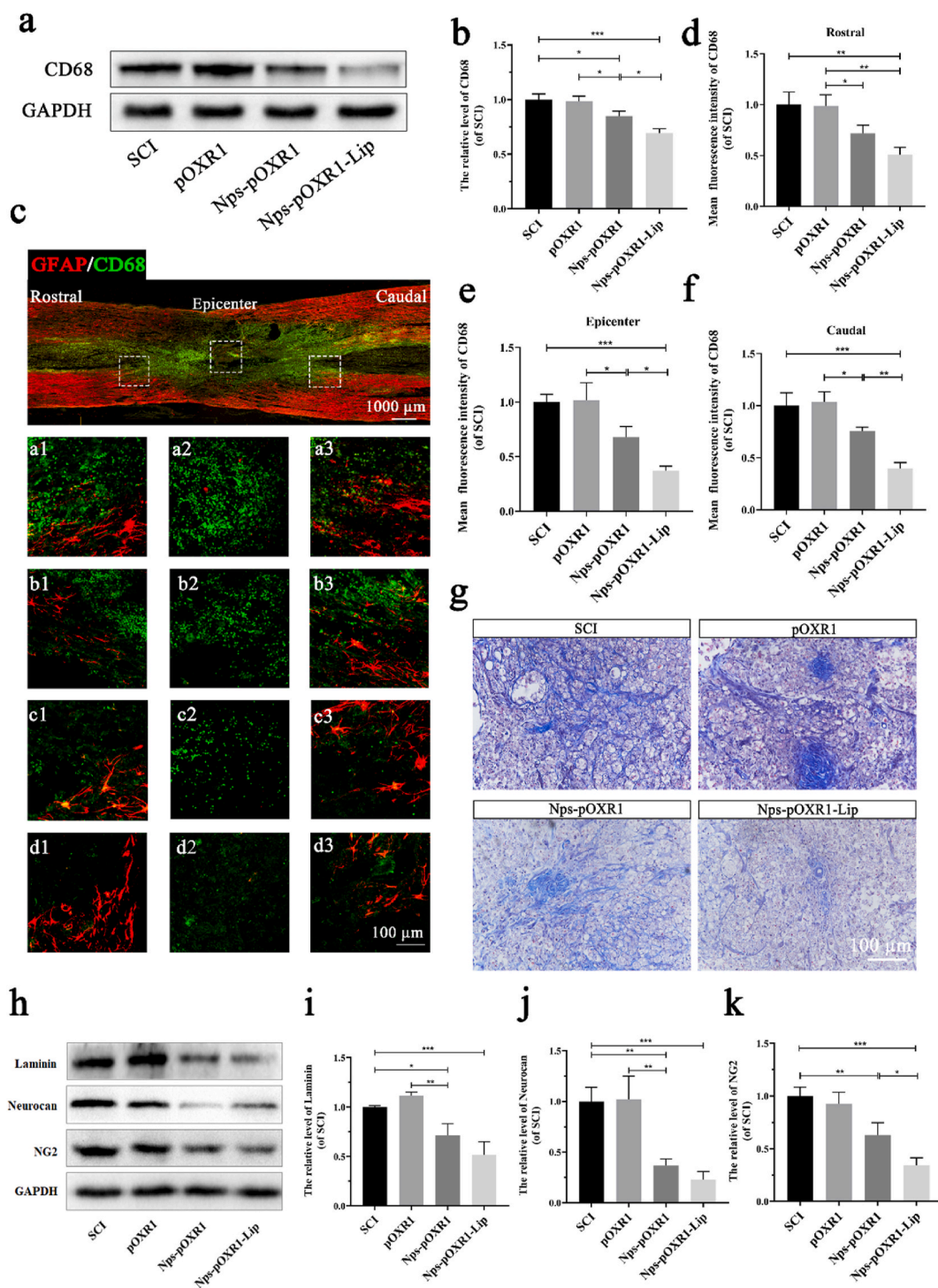


**Fig. 8.** Nps-pOXR1-Lip reduces fibrotic scar tissue by impacting the inflammatory reaction. (a–b) Immunoblot analysis showing protein expression levels of CD68 in various groups after 7 dpi (n = 3). (c–f) Immunofluorescence staining of monocytic phagocytes (CD68) and astrogliosis (GFAP) in spinal cord horizontal sections. Scale bar = 1000 μm. CD68-positive cells were detected in the rostral, epicentral and caudal sites of the spinal cord in the (a1–a3) SCI, (b1–b3) pOXR1, (c1–c3) Nps-pOXR1, and (d1–d3) Nps-pOXR1-Lip groups. Scale bar = 100 μm. (d–f) Fluorescence intensity quantification of CD68 in different sites. n = 3. (g) Masson staining of horizontal sections of spinal cord in various groups at 28 dpi. Scale bar = 100 μm. (h–k) Immunoblots and quantification of laminin, Neurocan, and NG2 expression in the spinal cord of various groups at 28 dpi. GAPDH was used as a loading control (n = 3). Data represent mean ± SD. n = 3. \*p < 0.05, \*\*p < 0.01, \*\*\*P < 0.001.

traumatic injury, behavior tests and histologic analysis were performed. In the current study, Nps-pOXR1-Lip was delivered immediately by a local injection after SCI (Fig. 5a). With Nps-pOXR1-Lip treatment, the spinal cord presented a relatively intact shape (Fig. 5b). In addition, the representative footprint analysis results indicated that rats that received Nps-pOXR1-Lip injection showed better recovery of hind leg movement with increased crawling after SCI (Fig. 5c). Furthermore, LFB staining also showed that the spinal cord lesion epicenter and its surroundings presented a smaller volume and exerted a pronounced effect on myelin sheath restoration (Fig. 5d), (Fig. 1c). Similar to the results of the above histological and behavioral tests, a 4-week period of BBB scores (Fig. 5e, g) and inclined plane tests (Fig. 5f, h) also suggested that Nps-pOXR1-Lip treatment enhanced BBB score and increased hindlimb strength compared to the SCI, pOXR1 and Nps-pOXR1 groups. Taken together, Nps-pOXR1-Lip contributes to functional recovery after SCI.

### 3.6. Nps-pOXR1-Lip attenuates neural apoptosis after SCI

As Nps-pOXR1-Lip was shown to present positive effects in promoting functional recovery, we accordingly evaluated whether Nps-pOXR1-Lip is sufficient to attenuate cell death after SCI. Initially, the TUNEL results showed that Nps-pOXR1-Lip treatment effectively reduced the number of TUNEL-positive cells after injury (Fig. 6a and b). In addition, IF staining colocalization of NEUN and cleaved caspase3 showed that Nps-pOXR1-Lip remarkably decreased the intensity of cleaved caspase3 in neurons (Fig. 6c and d). Consistent with the results of TUNEL and IF, western blot results showed that the Nps-pOXR1-Lip treatment group was associated with increased Bcl2 levels and decreased Bax and cleaved caspase3 expression (Fig. 6e–h). Similar to the western blot results, IF staining and TUNEL staining also indicated that Nps-pOXR1-Lip is a beneficial factor for protecting neurons from apoptosis.

### 3.7. Nps-pOXR1-Lip alleviates oxidative stress after SCI

Since oxidative stress is a common and critical pathologic process after SCI, we reasoned that Nps-pOXR1-Lip plays an important role in the regulation of redox reactions. DHE staining showed that Nps-pOXR1-Lip treatment obviously inhibited DHE intensity and reduced DHE-positive cells after injury (Fig. 7a and b). Subsequently, western blot analysis indicated that Nps-pOXR1-Lip treatment also increased the expression of Nrf2, HO-1, CAT and SOD1, both of which are critical enzymes related to protection against oxidative stress (Fig. 6c–g). Therefore, Nps-pOXR1-Lip is beneficial for the inhibition of oxidative stress.

### 3.8. Nps-pOXR1-Lip alleviates inflammation after SCI

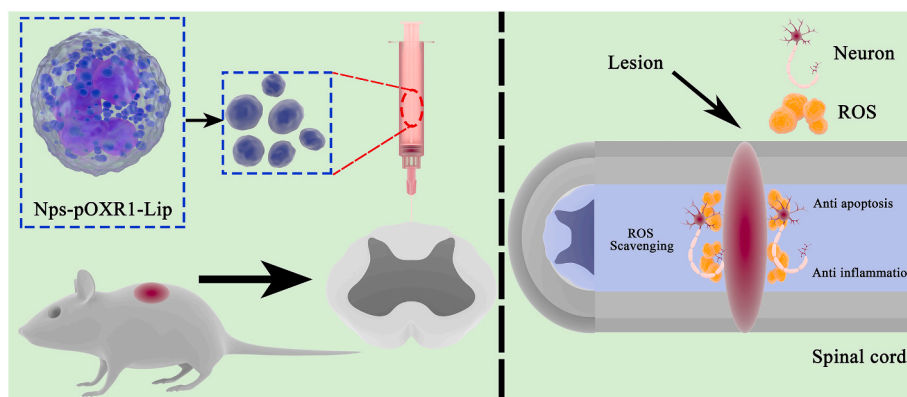
In addition, we determined the effect of Nps-pOXR1-Lip on neural inflammation after trauma. Western blot results showed, Nps-pOXR1-Lip remarkably reduced the level of CD68 expression, which is a common inflammatory marker in the spinal cord (Fig. 8a and b). In addition, IF showed that Nps-pOXR1-Lip attenuated the intensity of CD68 in the rostral, caudal and epicenter of injury in the spinal cord (Fig. 8c–f). The role of scar tissue in the lesion area after spinal cord injury is controversial [29,30]. However, fibrotic scarring with excessive expression of chemical inhibitors creates an environment that inhibits regeneration [31,32]. Masson staining showed collagen deposition in the lesion area. Nps-pOXR1-Lip significantly reduced collagen deposition and provided a suitable microenvironment for axon regeneration (Fig. 8g). In addition, Nps-pOXR1-Lip significantly decreased the levels of laminin, neurocan and NG2 (Fig. 8h–k). Thus, Nps-pOXR1-Lip effectively attenuates neural inflammation and inhibits scar formation after SCI.

## 4. Discussion

Gene therapy has been shown to be a viable strategy in neural repair strategies for central nervous system disorders, such as traumatic spinal cord injury (SCI) [33–35]. In the study, vitamin E succinate-grafted  $\epsilon$ -polylysine (VES-g-PLL) polymer cationic micelles were assembled and further encapsulated into liposomes for OXR1 plasmid loading and condensing. Correspondingly, pOXR1 was successfully encapsulated into the inner aqueous compartment of liposomes, and the liposomal nanoparticles exhibited good stability of particle size and effectively protected pOXR1 from DNase I degradation. Moreover, the nanoparticles significantly enhanced OXR1 expression in spinal cord neurons, which contributes to attenuating oxidative stress and neural apoptosis and improving functional recovery in SCI mice. Therefore, the designed Nps-pOXR1-Lip nanoparticle is a potential candidate for the management of SCI (Scheme 1).

Targeting oxidative stress inhibition is an important method in the treatment of SCI [36,37]. Oxidative stress is one of the common processes resulting from the release of large amounts of reactive oxygen species (ROS), and increased levels of ROS production have been closely related to the pathophysiology of SCI [38]. ROS can be classified according to its source, including mitochondrial electron transport chain and the nicotinamide adenine dinucleotide phosphate (NADPH) oxidase (NOX) family of enzymes. NOX as the main source of ROS which translocate to the membrane, where they generate ROS. The target of the drugs we delivered is the NOX-mediated ROS [39]. Firstly, this type of ROS plays an important role in pro-inflammation after spinal cord injury. Inhibition of NOX showed neuroprotective and anti-inflammatory effects [40]. The excessive ROS accumulation without treatment intervention could cause mitochondrial damage and release, which is responsible for apoptosis [41–43]. Numerous studies have suggested that attenuating oxidative stress using drugs or molecules of interest successfully promotes neural regeneration after SCI [44]. As a potentially potent regulator of oxidation, OXR1 has been investigated in various diseases in previous studies, the mechanism by which OXR1 regulates oxidative stress is an important issue. OXR1 has been presented as an upstream regulator of Mfn1, Mfn2, Drp1 and Fis1, all of which are critical factors for regulating mitochondrial shape and morphology. OXR1-mediated mitochondrial fusion regulator expression is a potential mechanism for attenuating cellular ROS accumulation [45]. Moreover, OXR1 is involved in regulating levels of Prdx2 oligomerization and its posttranslational modifications, suggested that OXR1 is a functional switch between the antioxidant and chaperone functions of Prdx2 [46]. In addition, loss of OXR1 results in autophagosomal or lysosomal deficits, and impaired autophagy causes ineffective removal of ROS [47]. Based on previous investigations, we speculated that OXR1-mediated antioxidant effects are associated with multiple mechanisms and processes.

Similar to a previous study, we found that OXR1 expression is increased in neurons and after SCI, suggesting that OXR1 is involved in the modulation of SCI and that overexpression of OXR1 is responsible for functional recovery. In neurons, OXR1 relieved oxidative stress by activation of the Nrf2/HO-1 pathway, which plays important roles in controlling ROS levels by regulating antioxidant enzymes [48]. We also observed that OXR1 was expressed in microglia. Typically, the damaged neurons release ROS, which functions as signaling molecules and activates glial cells, and then produce more reactive oxygen, active nitrogen, and pro-inflammatory mediators, which activates more glial cells and lead to further neuronal damage. The main function of OXR1 is increasing cellular resistance to ROS and the stress these molecules cause the cell [49]. Downregulation of OXR1 leads to microglial proliferation in the cerebellum and spinal cord [15]. Therefore, we hypothesize that OXR1 enhances the oxidation resistance of neuron and microglia. In this study, we mainly explored the protective role of OXR1 in neurons, as for its role in microglia, the deep mechanism need be further studied.



**Scheme 1.** The Nps-pOXR1-Lip nanoparticle is designed for treat SCI.

Since OXR1 is a protective molecule for SCI, improving the effect of OXR1 may be an essential issue for SCI treatment. In many previous studies, overexpressing molecules of interest with plasmids has been regarded as a prevalent and effective method for SCI treatment [50]. Consistent with these studies, the OXR1 plasmid was packaged and effectively enhanced neural OXR1 expression. However, gene therapy with simple liposome is inefficient because plasmids are unstable and cannot maintain relatively high concentrations. Nucleic acid compression could enhance the encapsulation efficiency and the stability of the DNA–cationic liposome complexes [51]. The particle size is one of the main factors that control the cytotoxicity and transfection efficiency of liposomes. Interestingly enough, the particle size of complexes could be reduced by pre-compression of nucleic acids [21]. As previous studies mentioned, PEI is a well-established biomaterial for plasmid loading, whereas several studies have indicated that PEI is associated with cytotoxicity under unsuitable dose injection [26]. Natural poly( $\epsilon$ -PLL) also can compress DNA, but the low permeability of cell membrane that limited its application [52]. Therefore, developing a vehicle for condensing the concentration and sustaining the stability of plasmids is a critical strategy for gene therapy. Unfortunately, the systematic comparison of liposomes in combination with these cationic polymers as delivery vectors has not been developed. More recently, our group developed a cationic micelle assembled with vitamin E succinate-grafted  $\epsilon$ -polylysine polymer and loaded with TRAIL plasmid, these polymers with a particle size of less than 30 nm and better permeability of cell membrane are likely to be effective vectors for therapeutic genes [19]. Herein, Nps-Lip loaded with OXR1 was assembled, and the results indicated that Nps-pOXR1-Lip significantly increased OXR1 expression in neurons and was identified as a safe carrier for OXR1 treatment for SCI.

The current study demonstrated that increasing OXR1 is an injury-inducible process in the adaptive response to SCI. Nps-pOXR1-Lip is an effective and safe method for promoting functional recovery and neuronal survival after SCI by inhibiting oxidative stress. Therefore, the presented evidence indicates that OXR1 exerts neuroprotection, and the assembled Nps-pOXR1-Lip appears to be an effective therapeutic method for acute traumatic SCI.

#### Ethics approval and consent to participate

All protocols and animal experiments were conducted in strict accordance with the Animal Care and Use Committee of Wenzhou Medical University (No. wydw-2018-0342).

#### Consent for publication

All contributing authors agree to the publication of this article.

#### Availability of data and materials

The datasets used and/or analyzed during the current study are available from the corresponding author on reasonable request.

#### CRediT authorship contribution statement

**Jing Zhang:** designed research and wrote the paper, guided experiment and picture performing; assisted in performing the experiment in vivo and in vitro; All authors read and approved the final manuscript. **Yao Li:** assisted in performing the experiment in vivo and in vitro; All authors read and approved the final manuscript. **Jun Xiong:** assisted in performing the experiment in vivo and in vitro; All authors read and approved the final manuscript. **Helin Xu:** guided experiment and picture performing; All authors read and approved the final manuscript. **Guanghen Xiang:** modified the syntax of paper; All authors read and approved the final manuscript. **Mingqiao Fan:** modified the syntax of paper; All authors read and approved the final manuscript. **Kailiang Zhou:** assisted in performing the experiment in vivo and in vitro; All authors read and approved the final manuscript. **Yutian Lin:** assisted in performing the experiment in vivo and in vitro; All authors read and approved the final manuscript. **Xiangxiang Chen:** assisted in performing the experiment in vivo and in vitro; All authors read and approved the final manuscript. **Lin Xie:** guided experiment and picture performing; All authors read and approved the final manuscript. **Hongyu Zhang:** modified the syntax of paper; All authors read and approved the final manuscript. **Jian Wang:** designed research and wrote the paper, assisted in designing research and approved the final version and submitted. All authors read and approved the final manuscript. **Jian Xiao:** designed research and wrote the paper, assisted in designing research and approved the final version and submitted. All authors read and approved the final manuscript.

#### Declaration of competing interest

The authors declare that they have no conflict of interests.

#### Funding and Acknowledgements

This work was supported by grants from Natural Science Foundation of China (81972150, 81772450, 81802251, 81801233), Natural Science Foundation of Zhejiang Province (LR18H50001, LQ18H090008). Research Unit of Research and Clinical Translation of Cell Growth Factors and Diseases of Chinese Academy of Medical Science (2019RU010).

## Appendix A. Supplementary data

Supplementary data to this article can be found online at <https://doi.org/10.1016/j.bioactmat.2021.03.001>.

## References

- I. Fischer, J. Dulin, M. Lane, Transplanting neural progenitor cells to restore connectivity after spinal cord injury, *Nat. Rev. Neurosci.* 21 (7) (2020) 366–383.
- K. Zhou, Z. Zheng, Y. Li, W. Han, J. Zhang, Y. Mao, H. Chen, W. Zhang, M. Liu, L. Xie, H. Zhang, H. Xu, J. Xiao, TFE3, a potential therapeutic target for Spinal Cord Injury via augmenting autophagy flux and alleviating ER stress, *Theranostics* 10 (20) (2020) 9280–9302.
- J. Kim, C. Mahapatra, J. Hong, M. Kim, K. Leong, H. Kim, J. Hyun, Functional recovery of contused spinal cord in rat with the injection of optimal-dosed cerium oxide nanoparticles, *Adv. Sci.* 4 (10) (2017) 1700034.
- S. Rao, Y. Lin, Y. Du, L. He, G. Huang, B. Chen, T. Chen, Designing multifunctionalized selenium nanoparticles to reverse oxidative stress-induced spinal cord injury by attenuating ROS overproduction and mitochondrial dysfunction, *J. Mater. Chem. B* 7 (16) (2019) 2648–2656.
- K. Suzuki, J. Elegeert, I. Song, H. Sasakura, O. Senkov, K. Matsuda, W. Kakegawa, A. Clayton, V. Chang, M. Ferrer-Ferrer, E. Miura, R. Kaushik, M. Ikeno, Y. Morioka, Y. Takeuchi, T. Shimada, S. Otsuka, S. Stoyanov, M. Watanabe, K. Takeuchi, A. Dityatev, A. Aricescu, M. Yuzaki, A synthetic synaptic organizer protein restores glutamatergic neuronal circuits, *Science* 369 (6507) (2020).
- W. Ong, C. Pinese, S. Chew, Scaffold-mediated sequential drug/gene delivery to promote nerve regeneration and remyelination following traumatic nerve injuries, *Adv. Drug Deliv. Rev.* (2019) 19–48.
- Y. Li, J. Zhang, K. Zhou, L. Xie, G. Xiang, M. Fang, W. Han, X. Wang, J. Xiao, Elevating Sestrin2 Attenuates Endoplasmic Reticulum Stress and Improves Functional Recovery through Autophagy Activation after Spinal Cord Injury, *Cell Biology and Toxicology*, 2020.
- S. Ilari, L. Giancotti, F. Lauro, M. Gliozzi, V. Malafoglia, E. Palma, M. Tafani, M. Russo, C. Tomino, M. Fini, D. Salvemini, V. Mollace, C. Muscoli, Natural antioxidant control of neuropathic pain-exploring the role of mitochondrial SIRT3 pathway, *Antioxidants* 9 (11) (2020).
- G. Jaramillo-Gutierrez, A. Molina-Cruz, S. Kumar, C. Barillas-Mury, The Anopheles gambiae oxidation resistance 1 (OXR1) gene regulates expression of enzymes that detoxify reactive oxygen species, *PLoS One* 5 (6) (2010) e11168.
- P. Oliver, M. Finelli, B. Edwards, E. Bitoun, D. Butts, E. Becker, M. Cheeseman, B. Davies, C. Davies, Oxr1 is essential for protection against oxidative stress-induced neurodegeneration, *PLoS Genet.* 7 (10) (2011), e1002338.
- E. D'Amico, P. Factor-Litvak, R. Santella, H. Mitsumoto, Clinical perspective on oxidative stress in sporadic amyotrophic lateral sclerosis, *Free Radical Biol. Med.* 65 (2013) 509–527.
- Y. Jiang, J. Liu, L. Chen, Y. Jin, G. Zhang, Z. Lin, S. Du, Z. Fu, T. Chen, Y. Qin, X. Sun, Serum secreted miR-137-containing exosomes affects oxidative stress of neurons by regulating OXR1 in Parkinson's disease, *Brain Res.* 1722 (2019) 146331.
- X. Zhang, S. Zhang, X. Liu, Y. Wang, J. Chang, X. Zhang, S. Mackintosh, A. Tackett, Y. He, D. Lv, R. Laberge, J. Campisi, J. Wang, G. Zheng, D. Zhou, Oxidation resistance 1 is a novel senolytic target, *Aging Cell* 17 (4) (2018), e12780.
- Y. Li, W. Li, C. Liu, M. Yan, I. Raman, Y. Du, X. Fang, X. Zhou, C. Mohan, Q. Li, Delivering oxidation resistance-1 (OXR1) to mouse kidney by genetic modified mesenchymal stem cells exhibited enhanced protection against nephrotoxic serum induced renal injury and lupus nephritis, *J. Stem Cell Res. Ther.* 4 (9) (2014).
- K. Liu, B. Edwards, S. Lee, M. Finelli, B. Davies, C. Davies, P. Oliver, Neuron-specific antioxidant OXR1 extends survival of a mouse model of amyotrophic lateral sclerosis, *Brain : J. Neurol.* 138 (2015) 1167–1181.
- Y. Xia, G. Tang, Y. Chen, C. Wang, M. Guo, T. Xu, M. Zhao, Y. Zhou, Tumor-targeted delivery of siRNA to silence Sox2 gene expression enhances therapeutic response in hepatocellular carcinoma, *Bioact. Mater.* 6 (5) (2021) 1330–1340.
- K. Hayakawa, S. Uchida, T. Ogata, S. Tanaka, K. Kataoka, K. Itaka, Intrathecal injection of a therapeutic gene-containing polyplex to treat spinal cord injury, *J. Contr. Release* 197 (2015) 1–9.
- T. Yang, C. Li, X. Wang, D. Zhao, M. Zhang, H. Cao, Z. Liang, H. Xiao, X. Liang, Y. Wang, Y. Huang, Efficient hepatic delivery and protein expression enabled by optimized mRNA and ionizable lipid nanoparticle, *Bioact. Mater.* 5 (4) (2020) 1053–1061.
- Y. Zhao, B. Shen, X. Li, M. Tong, P. Xue, R. Chen, Q. Yao, B. Chen, J. Xiao, H. Xu, Tumor cellular membrane camouflaged liposomes as a non-invasive vehicle for genes: specific targeting toward homologous gliomas and traversing the blood-brain barrier, *Nanoscale* 12 (28) (2020) 15473–15494.
- H. Xu, K. Mao, C. Lu, Z. Fan, J. Yang, J. Xu, P. Chen, D. ZhuGe, B. Shen, B. Jin, J. Xiao, Y. Zhao, An injectable acellular matrix scaffold with absorbable permeable nanoparticles improves the therapeutic effects of docetaxel on glioblastoma, *Biomaterials* 107 (2016) 44–60.
- J. Wang, X. Ye, H. Ni, J. Zhang, S. Ju, W. Ding, Transfection efficiency evaluation and endocytosis exploration of different polymer condensed agents, *DNA Cell Biol.* 38 (10) (2019) 1048–1055.
- H. Xu, Z. Fan, D. ZhuGe, B. Shen, B. Jin, J. Xiao, C. Lu, Y. Zhao, Therapeutic supermolecular micelles of vitamin E succinate-grafted  $\epsilon$ -polylysine as potential carriers for curcumin: enhancing tumour penetration and improving therapeutic effect on glioma, *Colloids Surf. B Biointerfaces* 158 (2017) 295–307.
- Z. Zheng, Y. Zhou, L. Ye, Q. Lu, K. Zhang, J. Zhang, L. Xie, Y. Wu, K. Xu, H. Zhang, J. Xiao, Histone deacetylase 6 inhibition restores autophagic flux to promote functional recovery after spinal cord injury, *Exp. Neurol.* 324 (2020) 113138.
- Q. Wang, H. Zhang, H. Xu, Y. Zhao, Z. Li, J. Li, H. Wang, D. Zhuge, X. Guo, H. Xu, S. Jones, X. Li, X. Jia, J. Xiao, Novel multi-drug delivery hydrogel using scar-homing liposomes improves spinal cord injury repair, *Theranostics* 8 (16) (2018) 4429–4446.
- S. Andrabi, J. Yang, Y. Gao, Y. Kuang, V. Labhasetwar, Nanoparticles with antioxidant enzymes protect injured spinal cord from neuronal cell apoptosis by attenuating mitochondrial dysfunction, *J. Contr. Release* 317 (2020) 300–311.
- S. Gwak, J. Nice, J. Zhang, B. Green, C. Macks, S. Bae, K. Webb, J. Lee, Cationic, amphiphilic copolymer micelles as nucleic acid carriers for enhanced transfection in rat spinal cord, *Acta Biomater.* 35 (2016) 98–108.
- L. Billiet, J. Gomez, M. Berchel, P. Jaffrès, T. Le Gall, T. Montier, E. Bertrand, H. Cheradame, P. Guégan, M. Mével, B. Pitard, T. Benvegnu, P. Lehn, C. Pichon, P. Midoex, Gene transfer by chemical vectors, and endocytosis routes of polyplexes, lipoplexes and lipopolyplexes in a myoblast cell line, *Biomaterials* 33 (10) (2012) 2980–2990.
- D. Patel, M. Santoro, L. Born, J. Fisher, S. Jay, Towards rationally designed biomaterials of therapeutic extracellular vesicles: impact of the bioproduction microenvironment, *Biotechnol. Adv.* 36 (8) (2018) 2051–2059.
- M. Anderson, J. Burda, Y. Ren, Y. Ao, T. O'Shea, R. Kawaguchi, G. Coppola, B. Khakh, T. Deming, M. Sofroniew, Astrocyte scar formation aids central nervous system axon regeneration, *Nature* 532 (7598) (2016) 195–200.
- J. Ruschel, F. Bradke, Systemic administration of epothilone D improves functional recovery of walking after rat spinal cord contusion injury, *Exp. Neurol.* 306 (2018) 243–249.
- K. Adams, V. Gallo, The diversity and disparity of the glial scar, *Nat. Neurosci.* 21 (1) (2018) 9–15.
- M. Condic, P. Letourneau, Ligand-induced changes in integrin expression regulate neuronal adhesion and neurite outgrowth, *Nature* 389 (6653) (1997) 852–856.
- E. Burnside, F. De Winter, A. Didangelos, N. James, E. Andreica, H. Layard-Horsfall, E. Muir, J. Verhaagen, E. Bradbury, Immune-evasive gene switch enables regulated delivery of chondroitinase after spinal cord injury, *Brain* 141 (8) (2018) 2362–2381.
- S. Gwak, C. Macks, D. Jeong, M. Kiny, M. Lynn, K. Webb, J. Lee, RhoA knockdown by cationic amphiphilic copolymer/siRhoA polyplexes enhances axonal regeneration in rat spinal cord injury model, *Biomaterials* 121 (2017) 155–166.
- D. Lou, Y. Luo, Q. Pang, W. Tan, L. Ma, Gene-activated dermal equivalents to accelerate healing of diabetic chronic wounds by regulating inflammation and promoting angiogenesis, *Bioact. Mater.* 5 (3) (2020) 667–679.
- P. Cheng, F. Kuang, G. Ju, Aescin reduces oxidative stress and provides neuroprotection in experimental traumatic spinal cord injury, *Free Radical Biol. Med.* 99 (2016) 405–417.
- M. Franco, Y. Ye, C. Refakis, J. Feldman, A. Stokes, M. Basso, R. Melero Fernández de Mera, N. Sparrow, N. Calingasan, M. Kiaei, T. Rhoads, T. Ma, M. Grumet, S. Barnes, M. Beal, J. Beckman, R. Mehl, A. Estévez, Nitration of Hsp90 induces cell death, *Proc. Natl. Acad. Sci. U. S. A.* 110 (12) (2013) E1102–E1111.
- N. Nukolova, A. Aleksashkin, T. Abakumova, A. Morozova, I. Gubskiy, E. Kirzhanova, M. Abakumov, V. Chekhonin, N. Klyachko, A. Kabanov, Multilayered polyion complex nanofibrillations of superoxide dismutase 1 for acute spinal cord injury, *J. Contr. Release* (2018) 226–236.
- S. Bermudez, G. Khayrullina, Y. Zhao, K. Byrnes, NADPH oxidase isoform expression is temporally regulated and may contribute to microglial/macrophage polarization after spinal cord injury, *Mol. Cell. Neurosci.* 77 (2016) 53–64.
- G. Fatima, V. Sharma, S. Das, A. Mahdi, Oxidative stress and antioxidative parameters in patients with spinal cord injury: implications in the pathogenesis of disease, *Spinal Cord* 53 (1) (2015) 3–6.
- W. Poewe, K. Seppi, C. Tanner, G. Halliday, P. Brundin, J. Volkmann, A. Schrag, A. Lang, Parkinson disease, *Nat. Rev. Dis. Prim.* 3 (2017) 17013.
- W. Hubbard, C. Harwood, J. Geisler, H. Vekaria, P. Sullivan, Mitochondrial uncoupling produg improves tissue sparing, cognitive outcome, and mitochondrial bioenergetics after traumatic brain injury in male mice, *J. Neurosci. Res.* 96 (10) (2018) 1677–1688.
- Y. Han, C. Gao, H. Wang, J. Sun, M. Liang, Y. Feng, Q. Liu, S. Fu, L. Cui, C. Gao, Y. Li, Y. Yang, B. Sun, Macrophage membrane-coated nanocarriers Co-Modified by RVG29 and TPP improve brain neuronal mitochondria-targeting and therapeutic efficacy in Alzheimer's disease mice, *Bioact. Mater.* 6 (2) (2021) 529–542.
- X. Chen, J. Cui, X. Zhai, J. Zhang, Z. Gu, X. Zhi, W. Weng, P. Pan, L. Cao, F. Ji, Z. Wang, J. Su, Inhalation of hydrogen of different concentrations ameliorates spinal cord injury in mice by protecting spinal cord neurons from apoptosis, oxidative injury and mitochondrial structure damages, *Cell. Physiol. Biochem.* 47 (1) (2018) 176–190, international journal of experimental cellular physiology, biochemistry, and pharmacology.
- Y. Wu, K. Davies, P. Oliver, The antioxidant protein Oxr1 influences aspects of mitochondrial morphology, *Free Radical Biol. Med.* 95 (2016) 255–267.
- D. Svistunova, J. Simon, E. Rembeza, M. Crabtree, W. Yue, P. Oliver, M. Finelli, Oxidation resistance 1 regulates post-translational modifications of peroxiredoxin 2 in the cerebellum, *Free Radical Biol. Med.* 130 (2019) 151–162.
- J. Wang, J. Rousseau, E. Kim, S. Ehresmann, Y. Cheng, L. Duraine, Z. Zuo, Y. Park, D. Li-Kroeger, W. Bi, L. Wong, J. Rosenfeld, J. Gleeson, E. Fageih, F. Alkuraya, K. Wierenga, J. Chen, A. Afenjar, C. Nava, D. Doummar, B. Keren, J. Juusola, M. Grompe, H. Bellen, P. Campeau, Loss of oxidation resistance 1, OXR1, is associated with an autosomal-recessive neurological disease with cerebellar atrophy and lysosomal dysfunction, *Am. J. Hum. Genet.* 105 (6) (2019) 1237–1253.

- [48] X. Yan, X. Fu, Y. Jia, X. Ma, J. Tao, T. Yang, H. Ma, X. Liang, X. Liu, J. Yang, J. Wei, Nrf2/Keap1/ARE Signaling Mediated an Antioxidative Protection of Human Placental Mesenchymal Stem Cells of Fetal Origin in Alveolar Epithelial Cells, *Oxidative Medicine and Cellular Longevity* 2019, 2019, p. 2654910.
- [49] M. Volkert, D. Crowley, Preventing neurodegeneration by controlling oxidative stress: the role of OXR1, *Front. Neurosci.* 14 (2020) 611904.
- [50] M. Zavvarian, A. Toossi, M. Khazaei, J. Hong, M. Fehlings, *Novel Innovations in Cell and Gene Therapies for Spinal Cord Injury*, F1000Research, vol. 9, 2020.
- [51] I. Ullah, J. Zhao, S. Rukh, K. Muhammad, J. Guo, X. Ren, S. Xia, W. Zhang, Y. Feng, A PEG-b-poly(disulfide-l-lysine) based redox-responsive cationic polymer for efficient gene transfection, *J. Mater. Chem. B* 7 (11) (2019) 1893–1905.
- [52] S. Hwa Kim, J. Hoon Jeong, C. Joe, T. Gwan Park, Folate receptor mediated intracellular protein delivery using PLL-PEG-FOL conjugate, *J. Contr. Release* 103 (3) (2005) 625–634, official journal of the Controlled Release Society.